Biomaterials 290 (2022) 121817

Contents lists available at ScienceDirect

Biomaterials

journal homepage: www.elsevier.com/locate/biomaterials

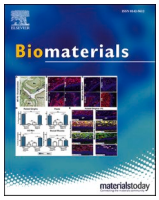

Modelling fatty liver disease with mouse liver-derived multicellular spheroids

Elise Anne van Os [a,1], Laura Cools [a,1], Nathalie Eysackers [a], Karolina Szafranska [b], Ayla Smout [a], Stefaan Verhulst [a], Hendrik Reynaert [a], Peter McCourt [b], Inge Mannaerts [a,2], Leo A. van Grunsven [a,*,2]

[a] Liver Cell Biology Research Group, Vrije Universiteit Brussel, Laarbeeklaan 103, 1090, Brussels, Belgium
[b] Vascular Biology Research Group, Department of Medical Biology, University of Tromsø (UiT) - the Arctic University of Norway, Tromsø, Norway

ARTICLE INFO

Keywords:
Liver fibrosis
Hepatic stellate cells
Hepatocytes
Liver sinusoidal endothelial cells
Kupffer cells
NAFLD
NASH
Liver spheroids
Drug screening

ABSTRACT

Chronic liver disease can lead to liver fibrosis and ultimately cirrhosis, which is a significant health burden and a major cause of death worldwide. Reliable *in vitro* models are lacking and thus mono-cultures of cell lines are still used to study liver disease and evaluate candidate anti-fibrotic drugs. We established functional multicellular liver spheroid (MCLS) cultures using primary mouse hepatocytes, hepatic stellate cells, liver sinusoidal endothelial cells and Kupffer cells. Cell-aggregation and spheroid formation was enhanced with 96-well U-bottom plates generating over ±700 spheroids from one mouse. Extensive characterization showed that MCLS cultures contain functional hepatocytes, quiescent stellate cells, fenestrated sinusoidal endothelium and responsive Kupffer cells that can be maintained for 17 days. MCLS cultures display a fibrotic response upon chronic exposure to acetaminophen, and present steatosis and fibrosis when challenged with free fatty acid and lipopolysaccharides, reminiscent of non-alcoholic fatty liver disease (NAFLD) stages. Treatment of MCLS cultures with potential anti-NAFLD drugs such as Elafibranor, Lanifibranor, Pioglitazone and Obeticholic acid shows that all can inhibit steatosis, but only Elafibranor and especially Lanifibranor inhibit fibrosis. Therefore, primary mouse MCLS cultures can be used to model acute and chronic liver disease and are suitable for the assessment of anti-NAFLD drugs.

1. Introduction

Chronic liver disease and cirrhosis are a significant public health threat worldwide [1]. The progression of fibrosis by chronic liver disease causes cirrhosis and increases the risk to develop hepatocellular carcinoma (HCC) [2]. Globally, liver cirrhosis accounts for 1.16 million deaths and accounts for 2% of all deaths [1]. Liver fibrosis and consequently cirrhosis can be caused by various underlying aetiologies such as viral hepatitis, non-alcoholic fatty liver disease (NAFLD), alcoholic-(ASH) and non-alcoholic-steatohepatitis (NASH) [2]. Currently, no therapies are available in the clinic that can target fibrosis directly, meaning that liver transplantation is the only therapeutic option for patients with end stage liver disease [2]. Research from the last decades has provided us with multiple targets for anti-fibrosis drug development [3]. Unfortunately, the numerous candidate drugs that have gone to clinical trials only have shown limited efficacy [2,4,5]. This highlights our incomplete understanding of the cellular mechanisms involved in liver fibrosis.

Key events in chronic liver disease are hepatocyte injury or death, liver sinusoidal endothelial cell (LSEC) dedifferentiation and hepatic stellate cell (HSC) activation. LSECs have a gatekeeper function as they promote HSC quiescence which is lost upon LSEC dedifferentiate and fibrosis [6]. Furthermore, the liver resident macrophages, known as Kupffer cells (KC) initiate an inflammatory response upon liver injury by the secretion of cytokines and chemokines and thereby stimulate HSC activation [7]. Current approaches to understand HSC activation are largely based on two-dimensional (2D) *in vitro* models of HSCs, which may have led to erroneous conclusions about their behaviour *in vivo* [8].

* Corresponding author. Laarbeeklaan 103, 1090, Jette, Belgium.
E-mail address: leo.van.grunsven@vub.be (L.A. van Grunsven).
[1] These authors share first authorship.
[2] These authors share last authorship.

https://doi.org/10.1016/j.biomaterials.2022.121817
Received 4 May 2022; Received in revised form 28 July 2022; Accepted 19 September 2022
Available online 28 September 2022

This has prompted the field to invest in the development of better *in vitro* and *in vivo* models of liver fibrosis for pre-clinical drug screening [9–11]. Advances in three-dimensional (3D) culture systems and tissue engineering, including the use of spheroid cultures and organ-on-a-chip models, have provided us with tools to better recapitulate the complex *in vivo* liver morphology and to study the interplay between parenchymal and non-parenchymal liver cells important for disease development, including processes of hepatocyte injury, inflammation, and fibrosis [12–14]. Although primary human cells would be the preferred source for all such 3D culture systems, there are important drawbacks that need to be considered. Primary human liver cells are scarce, need to be cryo-preserved [15], and show a high donor-variation. Moreover, human non-parenchymal cells (NPCs) are often passaged before use, resulting in activated/dedifferentiated liver cells [16]. Other potential sources are induced pluripotent stem cells (iPSC) or embryonic stem cells as an unlimited supply for hepatocytes and NPCs. Despite the tremendous efforts to improve the differentiation of these cells, iPSC-derived cells do not yet fully resemble the primary liver cell types [17–19]. The use of primary mouse liver cells, in combination with 3D culture techniques is still a valid option to facilitate and reduce the costs of screening of potential (anti-fibrotic) drugs and it will lower the use of mice for pharmacological testing which is in accordance with the 3R principle [20,21].

In this study, we established and extensively characterized a multicellular *in vitro* spheroid culture model using primary mouse hepatocytes, HSCs, LSECs and KCs as these cells play important roles in liver disease initiation and/or progression. Liver spheroids, formed and cultured in 96-well U-shaped cell-repellent plates for 17 days, maintain the independent liver cell functionalities and the capacity to mount a fibrotic response upon drug-induced liver damage or fatty liver

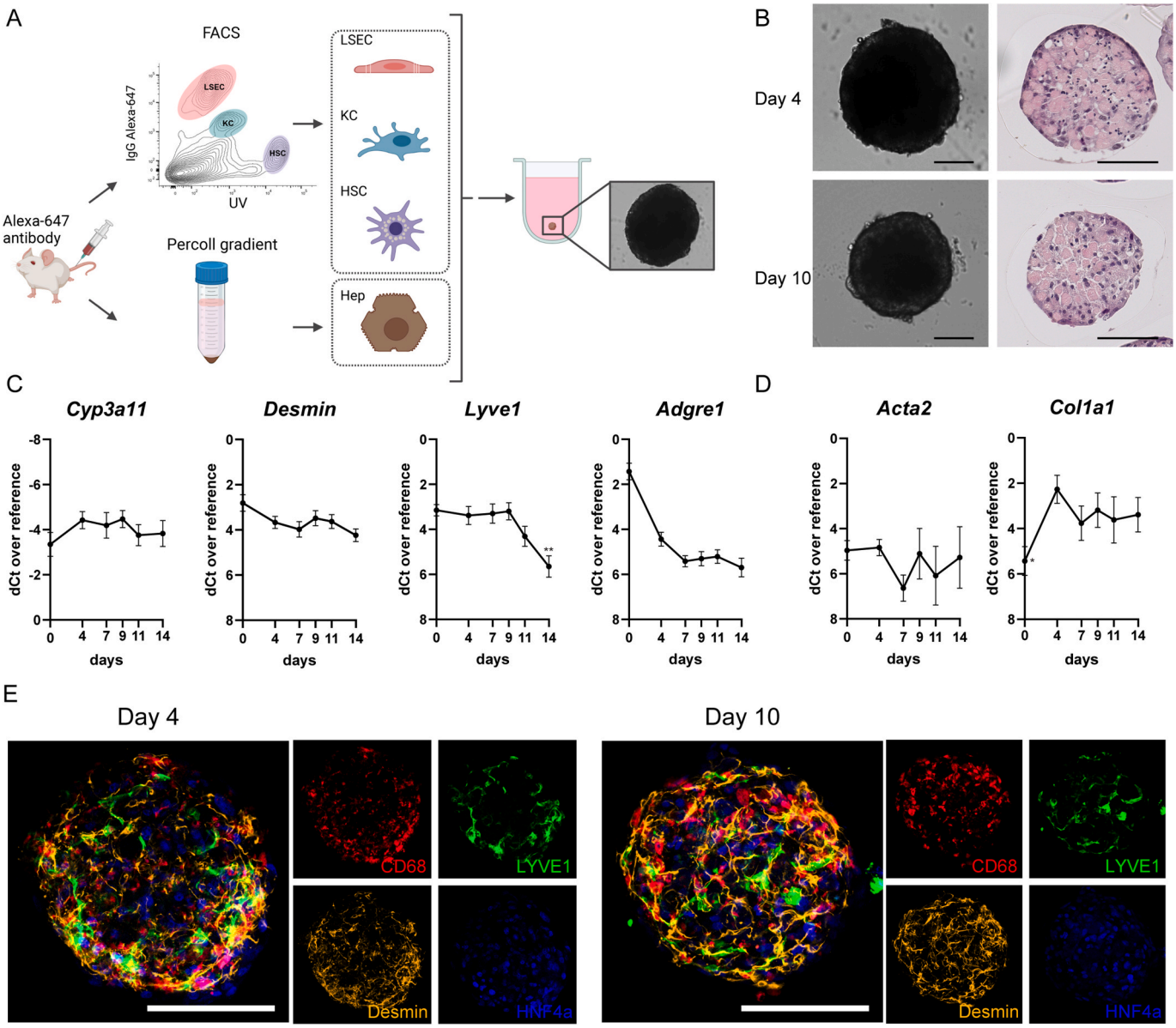

Fig. 1. Integration and maintenance of liver cells in MCLS cultures. (A) Setup of cell isolation and MCLS cultures. Cells were purified using UFACS [25] and a Percoll gradient, and subsequently plated in 96-well U-bottom cell-repellent plates. (B) Bright field images and Hematoxylin & Eosin staining of spheroids at day 4 and 10. (C) mRNA expression levels of cell specific markers *Cyp3a11* (Hepatocytes), *Desmin* (HSCs), *Lyve1* (LSEC) and *Adgre1* (KCs). Friedman test (one tailed) with all timepoints vs D4 $^{**}P \leq 0.01$ N = 7. (D) mRNA expression levels of HSC activation genes *Acta2* and *Col1a1* (N = 7). Friedman test (one tailed), all timepoints vs D4 $^{*}P \leq 0.05$. (E) Immunofluorescent staining of liver cell specific proteins HNF4α (Hepatocytes), Desmin (HSCs), LYVE1 (LSEC), CD68 (KCs) at day 4 and 10 of culture. Scale bar represents 100 μm.

conditions. Importantly, the anti-steatotic and anti-fibrotic efficacy of anti-NAFLD compounds such as Elafibranor, Lanifibranor and Obeticholic acid as observed in mice, could be reproduced in these cultures.

2. Results

2.1. Integration and maintenance of liver cells in multicellular liver spheroids cultures

Primary liver cells dedifferentiate and deteriorate rapidly upon 2D (mono)culture [22–24]. To circumvent this culture-induced dedifferentiation we established mouse multicellular liver spheroids (MCLS) using freshly isolated highly pure HSCs, KCs, LSECs and hepatocytes. All cells were isolated using a modified Ultraviolet fluorescence-activated cell sorting (UFACS) protocol [25] with small modifications that allows the isolation of viable hepatocytes (Percoll gradient) and FACS-sorted NPCs. From one mouse, up to ±700 MCLS can be cultured in 96-well U-bottom shaped cell-repellent plates with orbital shaking, resulting in cell aggregation and the formation of 200 μm diameter spheroids (Fig. 1A and B). Hematoxylin and eosin (H&E) staining shows

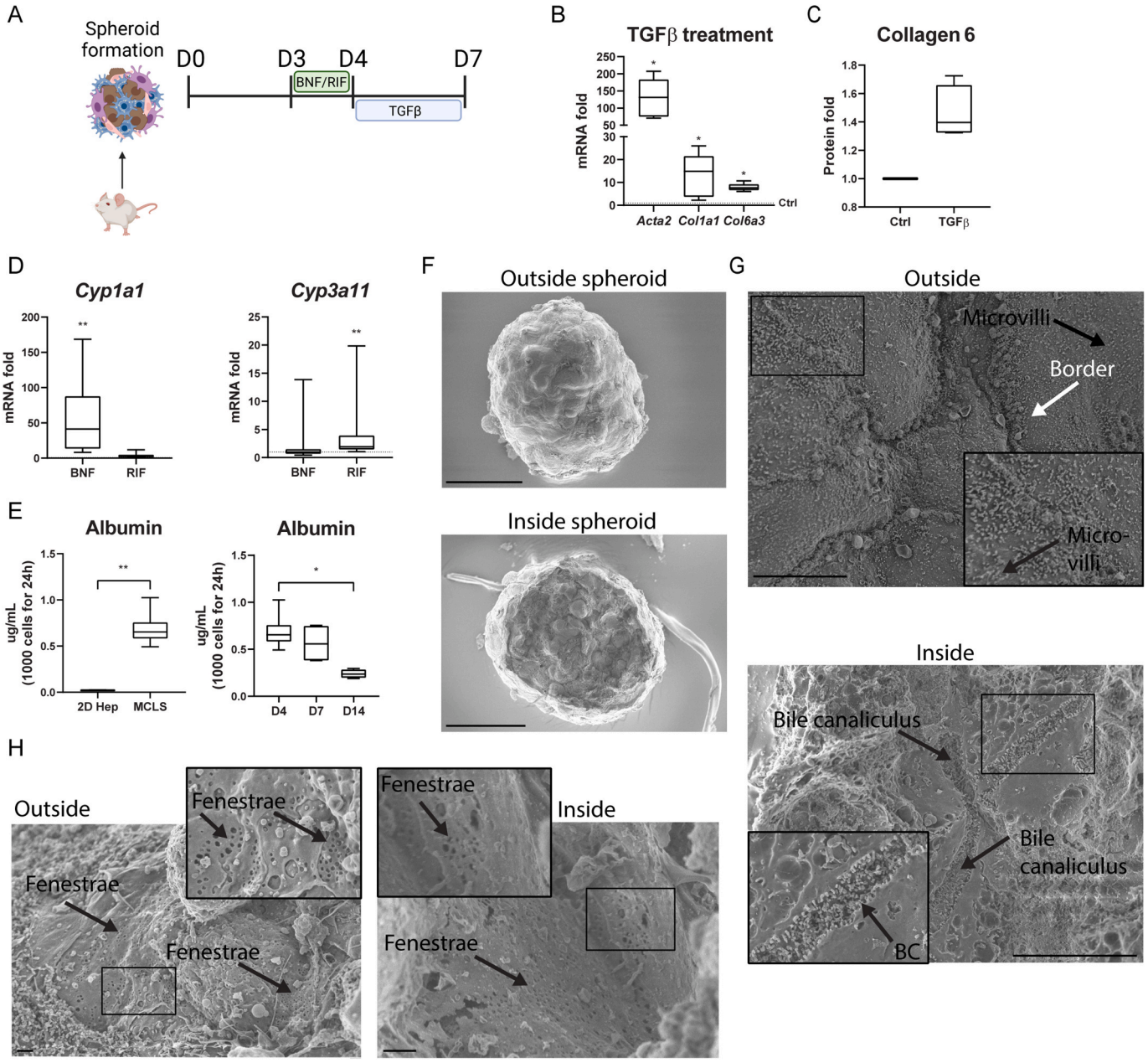

Fig. 2. Liver cell functionalities of Hepatocytes, HSCs, and LSECs in MCLS cultures. (A) Experimental setup of treatments. (B) mRNA expression of *Acta2*, *Col1a1* and *Col6a3* after 72 h TGFβ (10 ng/ml) exposure relative to control (Ctrl) (N = 6). Wilcoxon test (1 tailed), *P ≤ 0.05. (C) Collagen 6 secretion into the media after 72 h TGFβ (10 ng/ml) exposure relative to ctrl (N = 4), Wilcoxon test (1 tailed). (D) Induced mRNA expression of cytochrome P450 enzymes after the addition of CYP inducers BNF (25 μm) and RIF (10 μm) for 24 h to MCLS cultures at day 3 relative to control (N = 7). Friedmann test (one tailed), **P ≤ 0.01. (E) Albumin secretion measured in the media (ng/ml/1000 cells/24 h) in 2D hepatocytes at day 4 and 3D MCLS cultures at day 4, 7 and 14 (N = 6). Mann-Whitney test (left graph) or Kruskall-Wallis test (right graph), *P ≤ 0.05, **P ≤ 0.01. (F) SEM images of the outside and inside of spheroids at day 4. Scale bar represents 100 μm. (G) High magnification of SEM shows microvilli (black arrow) on hepatocytes, borders between hepatocytes (white arrow) at day 4 and bile canaliculi (BC, black arrow) at day 7 in the inside of the spheroids. Scale bar represents 10 μm. (H) SEM images of LSECs with fenestrae (black arrow) and sieve plates at the outside and inside of the spheroids at day 4. Scale bar represents 1 μm.

absence of a necrotic core and the scattered distribution of small and large nuclei indicating the presence of parenchymal and non-parenchymal cells (Fig. 1B). This morphology can be maintained for at least 17 days. Hepatocytes (*Cyp3a11*), HSCs (*Desmin*) and LSECs (*Lyve1*) integrate into a well-formed spheroid and remain present throughout the culture, with only a decline in *Lyve1* expression at the last days of culture (Fig. 1C). A suboptimal integration of KCs into the spheroids was demonstrated by the drop in *Adgre1* (F4/80) mRNA levels from day 0, representing the cell mixture used for seeding, to day 4 when the spheroid formation is complete (Fig. 1C). Primary mouse HSCs activate upon 2D culture which can be prevented by 3D cultivation of HSCs [24,26]. In the MCLS cultures, HSCs do not activate as shown by stable *Acta2* mRNA levels and only a slight upregulation of *Col1a1* after the first days of culture (Fig. 1D). Staining for liver cell specific proteins demonstrates a scattered distribution of all cell types in the MCLS and confirms the maintenance of these cell types over culture time (Fig. 1E, Supplementary Fig. 1).

2.2. Primary liver cell functionalities are preserved in MCLS cultures

Next, we evaluated the functionality of the incorporated cell types after establishing MCLS cultures (Fig. 2A). In an adequate model for chronic liver disease, HSCs should maintain the capacity to activate. In MCLS cultures, exposure to the pro-fibrogenic growth factor transforming growth factor beta (TGFβ) results in a strong activation of HSCs as shown by the increased expression of *Acta2, Col1a1* and *Col6a3* in the spheroids and an induction of Collagen 6 protein in the culture medium (Fig. 2B and C). Phase 1 metabolic capacity of the integrated hepatocytes was shown by exposure to cytochrome P450 (CYP) inducers β-naphthoflavone (BNF) and Rifampicin (RIF) resulting in higher mRNA levels of *Cyp1a1* and *Cyp3a11* (Fig. 2D). In addition, high and sustained albumin production was measured in the media illustrating the maintenance of functional hepatocytes in the MCLS cultures (Fig. 2E). Albumin secretion of MCLS cultures is higher (>32x at day 4) at all timepoints in comparison to 2D hepatocytes cultured for 4 days. Furthermore, scanning electron microscopy (SEM) images of the spheroids show the presence of microvilli on hepatocytes and bile canaliculi between hepatocytes (Fig. 2F and G). These images also show smooth cells at the surface of the spheroids with small cytoplasmatic pores that can be identified as fenestrae clustered together in sieve plates (Fig. 2H), the golden standard for identification and demonstration of the health status of LSECs [27]. The inside of spheroids displays small cavities lined with smooth cells and fenestrae both on day 4 (Fig. 2H) and day 7 (Suppl. Fig. 2) which suggests that LSECs retain their phenotype in MCLS cultures.

To evaluate the functionality of the KCs in the MCLS, we hypothesized that spheroids could induce an inflammatory response through KCs. To this end, spheroids with and without KCs were exposed for 72 h to lipopolysaccharide (LPS), a strong ligand for Toll like receptor 4 expressed on KCs [28], HSCs [29] and to a lower extend on LSECs [30] and hepatocytes [31] (Fig. 3A). Only in MCLS with KCs, LPS exposure results in a high increase of *IL-1β* and *TNFα* mRNA expression demonstrating a higher inflammatory response in the presence of KCs (Fig. 3B). Moreover, the addition of LPS also led to a modest but significant HSC activation when KCs were incorporated, as demonstrated by the increase of *TGFβ* and *Col1a1* mRNA levels (Fig. 3C). Further analysis of secreted proteins showed an increased cytokine release of IL-6 and TNFα into the media when KC-containing spheroids were stimulated with LPS (Fig. 3D), suggesting that KCs are the main producers of these cytokines in the MCLS cultures. In contrast, LPS-induced MCP1 protein release did not depend on KC presence and is probably released by the HSCs upon LPS exposure [32] (Fig. 3D). Finally, HSC activation was only significantly induced when Il-1β alone, or in combination with TNFα, was added to the MCLS with KCs (Fig. 3E), demonstrating that LPS can lead to an increased production of cytokines by KCs which in turn can lead to HSC activation. Taken together, these results demonstrate that primary mouse cells cultured as MCLS maintain their liver cell specific functionalities and that these cultures can be used to evaluate cellular crosstalk.

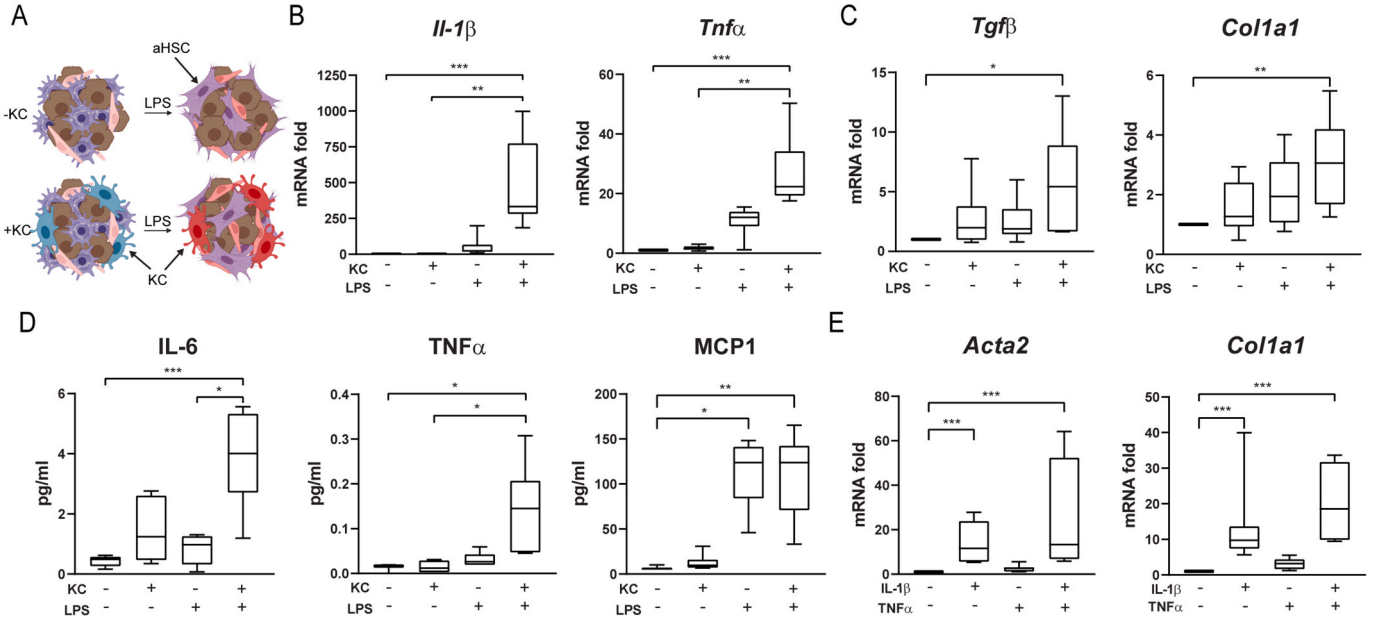

Fig. 3. KCs inflammatory properties in MCLS cultures. (A) Experimental setup of MCLS cultures and LPS treatment (HSCs – activated HSC). (B) Expression of inflammatory genes *Il-1β* and *TNFα* in MCLS cultures with or without KC exposed to LPS (100 ng/ml) for 72 h (N = 7). Friedman test (one tailed), **P ≤ 0.01, ***P ≤ 0.001 (C) mRNA expression of *TGFβ* and *Col1a1* in MCLS cultures with or without KC exposed to LPS (100 ng/ml) for 72 h (N = 6). Friedman test (one tailed), *P ≤ 0.05, **P ≤ 0.01 (D) Cytokines IL-6, TNFα and MCP1 measured in conditioned media in MCLS culture with or without KC exposed to LPS (100 ng/ml) for 72 h (N = 6). Kruskall-Wallis test (one-tailed, TNFα), Friedman test (one tailed, IL-6 and MCP1), *P ≤ 0.05, **P ≤ 0.01, ***P ≤ 0.001 (E) mRNA expression of *Acta2* and *Col1a1* in MCLS cultures treated with cytokines IL-1β (50 ng/ml) and TNFα (100 ng/ml)(N = 4–6). ***P ≤ 0.001.

2.3. Hepatocyte-damage induced HSC activation in MCLS cultures

Acetaminophen (APAP) was chosen to induce hepatotoxicity in the MCLS cultures. Long term treatment of APAP in mice leads to HSC activation and fibrosis [33,34]. To mimic chronic liver injury, we exposed spheroids for 3 days to 1.25 mM APAP (Fig. 4A). APAP exposure led to a drop in adenosine triphosphate (ATP) content (Fig. 4B) and ruffling of the spheroids indicative of hepatocyte injury (Fig. 4C). In addition, this hepatocyte damage leads to HSC activation as measured by *Acta2*, *Col1a1 and Col6a3* mRNA levels (Fig. 4D). Furthermore, APAP- exposed MCLS show a higher deposition of Collagen 1 in the spheroids and a higher secretion of Collagen 6 in the media (Fig. 4E and F). Taken together these results demonstrate that chronic exposure of MCLS with APAP generates a hepatocyte-damage induced HSC activation, thus mimicking a fibrotic response to hepatocyte injury.

2.4. NAFLD and NASH conditions result in steatosis, inflammation and HSC activation in MCLS cultures

We demonstrated that the MCLS were able to mimic a fibrotic phenotype after exposure to APAP (Fig. 4). Next, we investigated whether we could use these liver spheroids to model NAFLD and NASH. Free fatty acids (FFA) play an important role in the development of NAFLD and NASH, with oleic acid and palmitic acid being the most important contributors [35–37]. A NAFLD condition was created by incubating spheroids for 10 days with a mixture of oleic acid and palmitic acid (FFA) (Fig. 5A). For NASH induction, spheroids were treated with FFA rich media and supplemented with LPS for the last 72 h (Fig. 5A). Bright field images show smooth spheroids at day 17 of culture with no difference between treatment groups (Fig. 5B). The absence of a necrotic core in all treatment groups indicates that there is no massive cell death after 10 days of exposure to FFA (±LPS). More importantly, under both NAFLD and NASH conditions some cells show signs of ballooning and possible uptake of lipids indicated by a lighter colour of the cytoplasm and a clear enlarged cell volume (Fig. 5B, arrows). The lipid accumulation was confirmed with BODIPY staining (Fig. 5B, E). Interestingly, we found that treatment with FFA alone results in a small but non-significant increase of HSC activation genes (*Acta2*, *Col1a1* and *Lox*) but no induction of inflammatory markers (*Il-1β* and *TNFα*) (Fig. 5C and D). This response, together with the intrahepatic lipid accumulation, is indicative for a NAFLD-like phenotype. However, when FFA are combined with LPS, this results in a significant increase of HSC activation markers and inflammatory genes when compared to spheroids treated with either FFA or LPS alone (Fig. 5C and D) indicating the

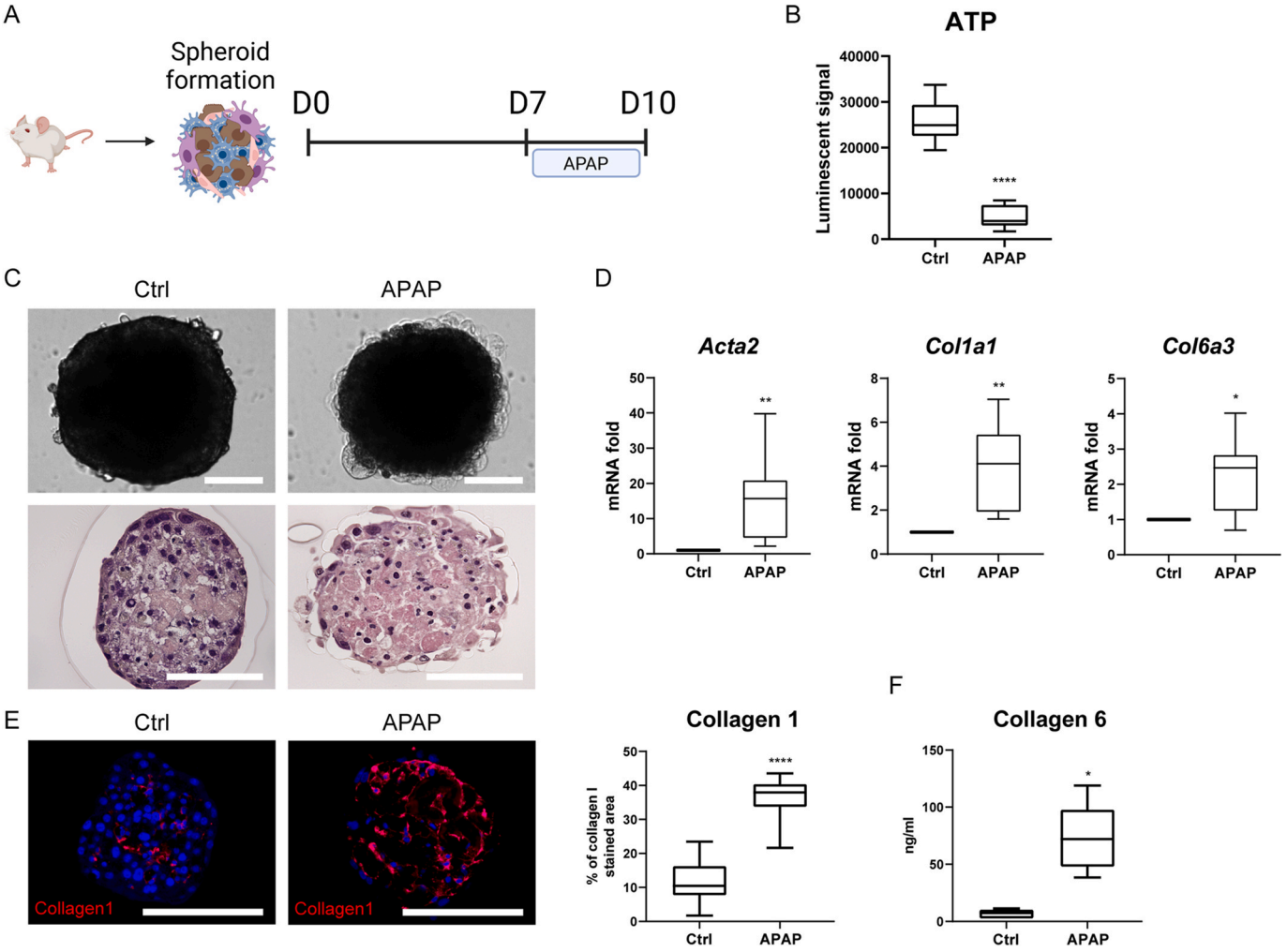

Fig. 4. Induction of hepatotoxicity induces a fibrotic response in MCLS. (A) Experimental setup for the induction of fibrosis with APAP. (B) ATP content measured in individual spheroids upon 3-day exposure with 1,25 mM APAP (N = 12). Wilcoxon test (1 tailed), ****P ≤ 0.0001. (C) Bright field images and H&E stains of control (Ctrl) and APAP treated MCLS. Scale bar represents 100 μm. (D) mRNA expression of Acta2, Col1a1 and Col6a3 after APAP treatment (1.25 mM) relative to untreated spheroids (N = 7). Wilcoxon test (1 tailed), *P ≤ 0.05, **P ≤ 0.01 (E) Collagen 1 staining of Ctrl and APAP-treated MCLS with quantification (N = 11). Scale bar represents 100 μm. Mann-Whitney (one-tailed), ****P ≤ 0.0001. (F) Collagen 6 secretion (ng/ml) by MCLS in Ctrl and APAP conditions (N = 5). Wilcoxon test (1 tailed), *P ≤ 0.05.

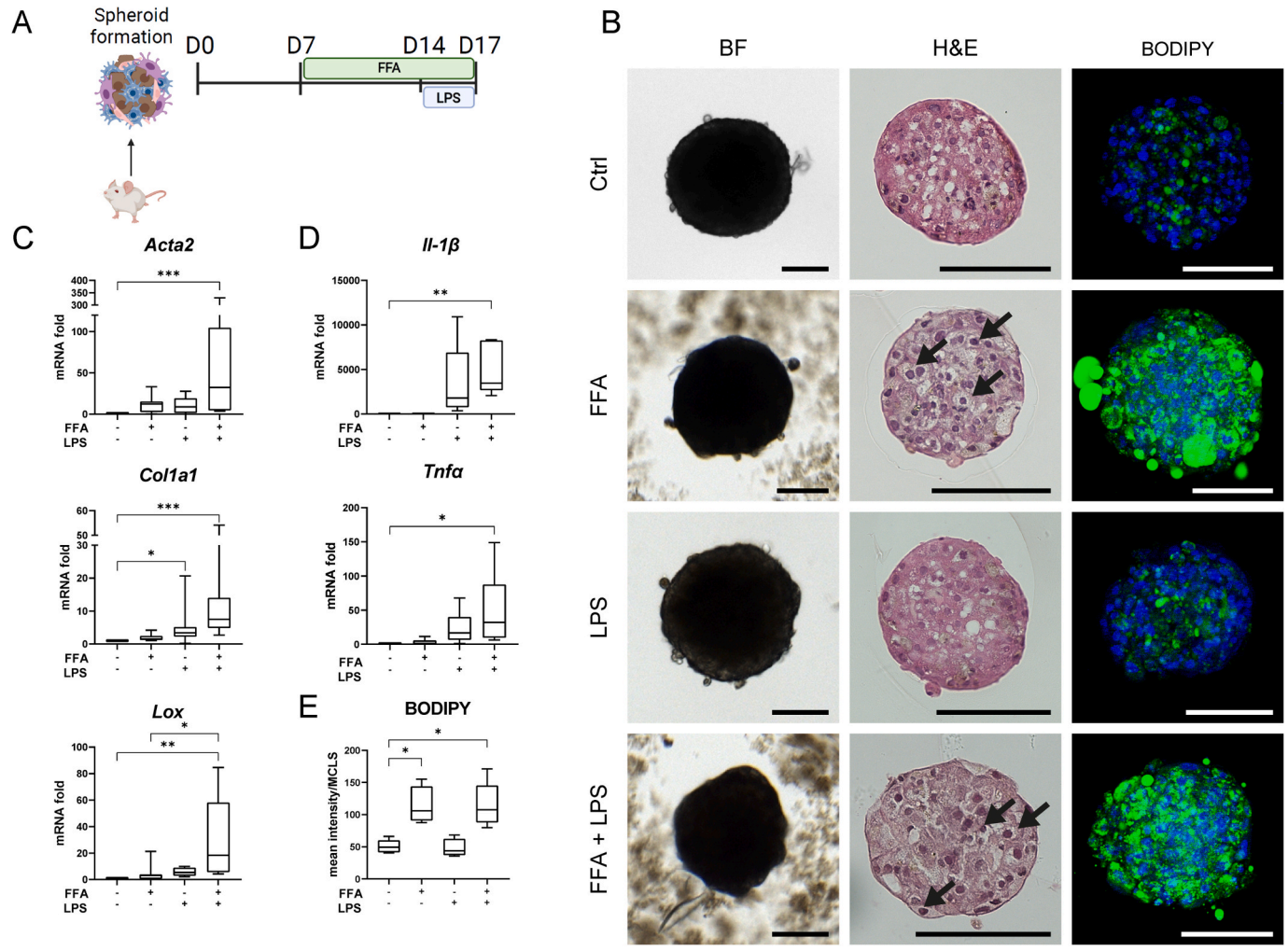

Fig. 5. NAFLD and NASH induction in MCLS. (A) Experimental setup for the induction of NAFLD and NASH in MCLS. (B) Bright field, Hematoxylin and Eosin staining and BODIPY immunofluorescent staining of control (Ctrl), LPS (100 ng/ml), FFA (400 μM oleic acid and 500 μM palmitic acid) and FFA + LPS treated spheroids after 10 days treatment. Nuclei were stained with DAPI. Scale bar represents 100 μm. Arrows indicate an enlarged cell volume. Images are representative of 3 independent experiments. (C) mRNA expression of HSC activation genes *Acta2*, *Col1a1* and *Lox* (D) mRNA expression of inflammatory genes *Il-1β* and *TNFα*. Friedman test (one tailed) with *P ≤ 0.05, **P ≤ 0.01, ***P ≤ 0.001 and N = 9. (E) Quantification of BODIPY staining of Ctrl, LPS, FFA and FFA + LPS treated spheroids (N = 5–8 spheroids of 2 different cultures). Kruskal-Wallis test (one tailed) with *P ≤ 0.05.

co-stimulatory effect of FFA with LPS. Overall, this suggests that MCLS exposed to combined FFA and LPS treatment show specific characteristics of a NASH phenotype.

2.5. Efficacy of anti-NAFLD compounds in MCLS cultures

Next, we evaluated whether MCLS cultures can be used to test potential anti-NAFLD/NASH drugs. First, we investigated if lipid accumulation can be prevented by treating MCLS in NAFLD conditions with drugs currently in clinical trials for the treatment of NAFLD and NASH. We examined the effect of peroxisome proliferator-activated receptor (PPAR) agonists Elafibranor (PPARα,δ) [38,39], Lanifibranor (pan-PPAR) [40], Pioglitazone (PPARγ) [40], the apoptosis signal-regulating kinase 1 (ASK1) inhibitor Selonsertib [41] and the farnesoid X receptor (FXR) agonist Obeticholic acid (OCA) [42] on FFA uptake in MCLS cultures (Fig. 6A). As expected, we found that Elafibranor, Lanifibranor and Pioglitazone were able to prevent lipid uptake, as they are PPAR agonists and directly target the uptake and metabolization of FFA. OCA was also able to reduce intracellular fat accumulation. Selonsertib treatment only slightly decreased the lipid uptake in the MCLS cultures (Fig. 6B and C). We further assessed the capacity of these drugs to resolve fibrosis formation in NASH conditions. Drugs were administered to NASH spheroids 24 h after LPS stimulation and spheroids were analyzed 48 h later (Fig. 6D). Only Elafibranor and Lanifibranor significantly reduced protein expression levels of Collagen 1 in the NASH conditions (Fig. 6E, G). These findings were not reflected by a significant downregulation of HSC activation markers at the mRNA level, only a trend could be observed (Suppl Fig. 3). BODIPY staining in these conditions showed no significant reduction in lipid accumulation when NASH spheroids were treated with compounds for the last 48 h (Fig. 6 F, H). These findings demonstrate that although most drugs can prevent lipid accumulation in these liver spheroid cultures, only Lanifibranor and Elafibranor significantly decreased Collagen accumulation in NASH conditions.

3. Discussion

Development of cell culture models that mimic organs such as the liver has made great progress since the field shifted from 2D mono-layer and single cell-type cultures to 3D spheroid/organoid cultures [43]. In general, cells (co-)cultured in suspension or hydrogels show a better functionality than cells cultured on hard plastic surfaces. For liver cultures, another challenge currently lies in the source of the liver cells; human primary cells are scarce and have a high inter-variability [15,16]

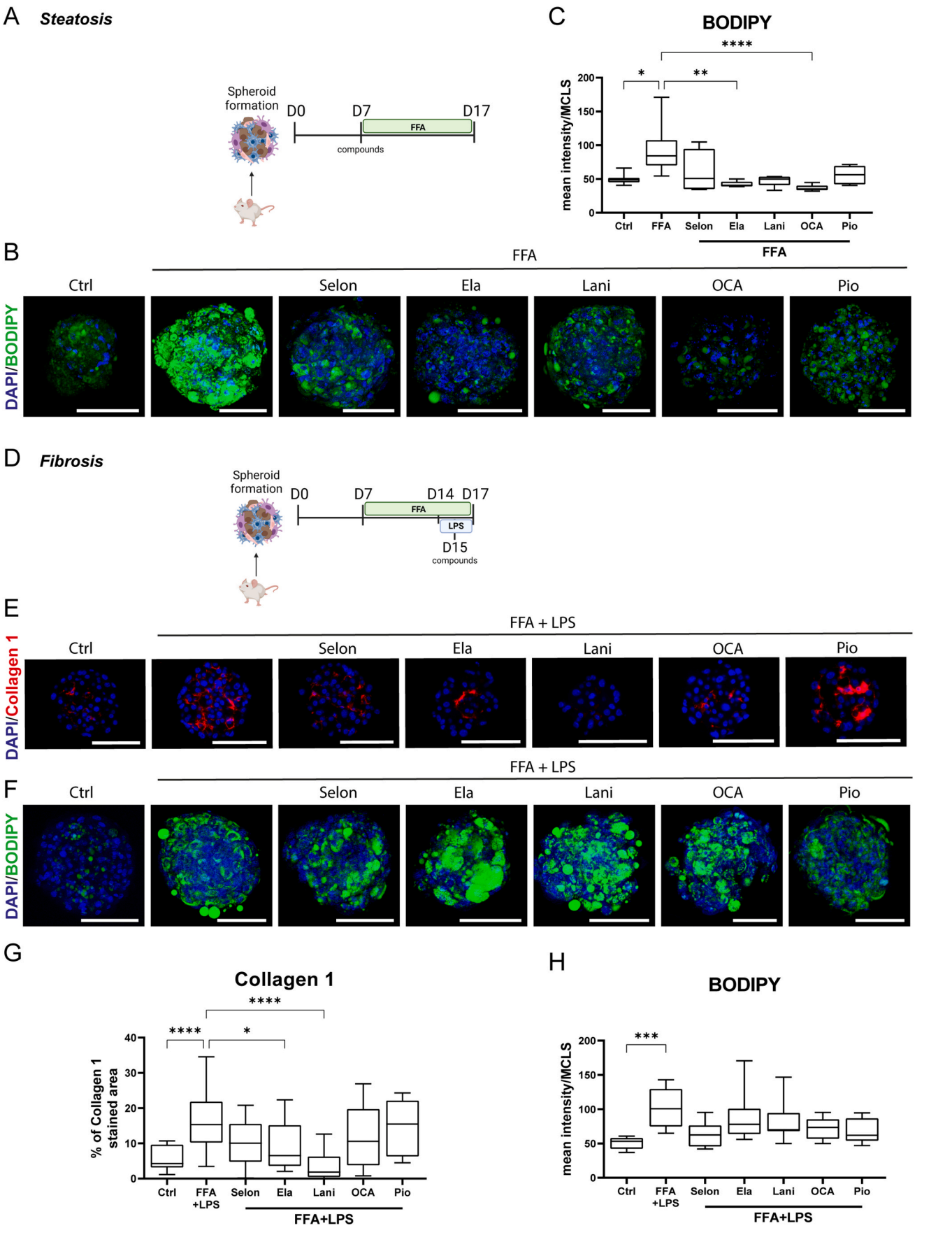

(caption on next page)

Fig. 6. Preventive and resolutive effect of anti-NAFLD/NASH compounds in NAFLD and NASH MCLS. (A) Experimental setup for preventive effect of Selonsertib (Selon), Elafibranor (Ela), Lanifibranor (Lani), Obeticholic acid (OCA) and Pioglitazone (Pio) in NAFLD MCLS. (B) Neutral lipid staining with BODIPY in NAFLD MCLS treated with the compounds for 10 days. Scale bar represents 100 μm. (C) BODIPY quantification of NAFLD spheroids treated with the indicated compounds for 10 days (N = 5–10 spheroids). Kruskal-Wallis (one tailed) with *P ≤ 0.05, **P ≤ 0.01, ****P ≤ 0.0001 (D) Experimental setup for anti-fibrotic effect of the compounds in NASH treated MCLS. (E) Collagen 1 and (F) BODIPY staining on NASH MCLS treated with compounds for 48 h. Nuclei were stained with DAPI. Scale bar represents 100 μm. (G) Quantification of Collagen 1 staining in NASH MCLS treated with the indicated compounds (N = 5–10 for each condition and 3 individual cultures), Kruskal-Wallis (one tailed) with *P ≤ 0.05, ****P ≤ 0.0001. (H) BODIPY quantification of NASH MCLS treated with Selonsertib, Elafibranor, Lanifibranor, Obeticholic acid and Pioglitazone for 48 h (N = 2–4), Kruskal-Wallis (one tailed) with ***P ≤ 0.001.

while iPSC-derived liver cells do not yet fully represent the endogenous liver [19]. In this study, we used primary mouse liver cells and established a robust 3D spheroid culture model and demonstrated their functionality by modelling drug induced liver injury, fibrosis, NAFLD and NASH. Most importantly, anti-NAFLD drugs showed similar efficacy in NAFLD and NASH spheroids as has been previously demonstrated in rodent studies [38–41,44]. Together, these results demonstrate that primary mouse liver derived spheroid cultures are a reliable and reproducible model to study mechanisms of liver disease and evaluate drugs against chronic liver disease.

One strength of the approach used here is the isolation and use of both hepatocytes and non-parenchymal cells from the same animal. Typically, parenchymal and non-parenchymal cells are isolated with different protocols and therefore multiple mice are needed. Here, a Percoll gradient was used [45] for hepatocytes and the UFACS3 methodology reported by Stradiot et al. [25,26] for LSECs, KCs and LSECs. This method enables the quick isolation of liver cells from multiple mice in parallel in one day. This also allows to pair parenchymal and non-parenchymal cells from different mice. This results in animal reduction, an important pillar of the 3R principal. One can obtain approximately 600–800 spheroids from one mouse liver, depending on the age of the mice; in our hands, at a young age (<15 weeks) KCs are limiting while at older age (>20 weeks) the HSC numbers are limiting.

The use of these highly pure and freshly isolated cells results in a stable long-term MCLS culture. Even though *Lyve1* mRNA levels tend to decline at later timepoints, which could indicate LSEC dedifferentiation, we do not observe a reduction of LSECs when stained for LYVE1. In addition, SEM images showed that LSECs in these cultures retain their fenestrae for at least 4 days, and probably longer since we could still visualize fenestrae at day 7, albeit to a lesser extent. To our knowledge, this is the first time that fenestrated LSECs are shown in 3D cultures, opening up new avenues to study processes and cellular interactions that can impact (de)fenestration of LSECs. Hepatocytes in the MCLS cultures are metabolically active (Cyp induction, albumin secretion) and morphologically intact (microvilli and bile canaliculi). If we compare these results to similar cultures recently reported by Nudischer et al., 2020 [46] the albumin secretion in the MCLS culture is considerably higher at day 4 (~3 times) and day 7 (~2 times) but lower at day 14 (~2 times) indicating that the quality of our isolated hepatocytes is high but does not increase after 2 weeks as reported by Nudischer et al.,. 2020. Successfully integrated KCs proved to be functional as only in the presence of KCs, LPS-induced IL-6 and TNFα proteins were secreted by the spheroids. In contrast, MCP1 protein production was clearly independent on the presence of KCs but rather rely on HSCs, confirming transcriptome studies from Bonnardel et al., 2019 and Kolodziejczyk et al., 2020, showing that HSCs are an important source of MCP1 for the attraction of monocytes [47,48]. We also found that HSC activation was the highest when KCs and LPS were present, indicating cellular communication between KCs and HSCs in these cultures. These results advocate the importance of multiple cells types in an *in vitro* model. Moreover, it shows the flexibility of the culture setup in which we control the cell type and amount of highly pure primary liver cells incorporated into the spheroids.

A shortcoming of this culture system is the 1:4 hepatocyte:NPC ratio, which does not resemble the *in vivo* situation in which a mouse liver contains 35–40% hepatocytes, or a 3:5 hepatocyte:NPC ratio [49]. The cellular ratio of the MCLS culture used found its origin in initial experiments with hepatocyte:HSC spheroids in which spheroid formation and hepatocyte functionality over culture time determined the currently used setup [26,33]. The current ratio allows a quick spheroid assembly without using additional Collagens or gels and, in our hands, results in stable functional cultures. This is supported by well functional hepatocytes, evident when challenged with APAP. The APAP concentration (1.25 mM) that was used to damage the MCLS cultures is under the Cmax of mice (2.2 mM which resulted from APAP treatment close to the median lethal dose (LD_{50}) of mice [50]). As demonstrated previously *in vivo* [33], APAP-induced hepatocyte injury and death resulted in an evident fibrotic response in these spheroids as well. More importantly, not only hepatocyte cell death, but also NASH conditions could induce a fibrotic response in the MCLS cultures. Both oleic and palmitic acid have previously been described as important key players in the onset of steatosis [51]. Addition of LPS to the NAFLD conditions mimicked the 'two hit' effect [52] and resulted in a significant increase in HSC activation and Collagen production. We also demonstrated that all three PPAR agonists and OCA can inhibit lipid accumulation in the MCLS cultures, which correlates with findings in a diet induced NASH model [53]. However, only Lanifibranor and Elafibranor were able to reduce fibrosis. Our findings correspond to the effects of Elafibranor and Lanifibranor obtained in NASH mice where both compounds reduced fat accumulation and fibrosis [54,55]. In contrast, Pioglitazone, which could reduce steatosis in the spheroids, did not reduce fibrosis. Clinical trials with Pioglitazone reported similar effects; a reduction in steatosis and inflammation, but no change in fibrosis [56]. For Selonsertib, we only observed a small non-significant reduction of fat accumulation in our NAFLD model but demonstrated a trend towards a reduction on fibrosis in the NASH model corresponding to *in vivo* obtained data where Selonsertib was able to reduce fibrosis in a murine NASH model [57]. Even though an *in vitro* mouse model does not seem directly relevant for drug testing we would like to emphasize that a rodent *in vitro* equivalent can contribute greatly to drug development as animal models are still the preferred intermediate step from *in vitro* findings to clinical trials. The MCLS cultures presented here can be used to predict the effect of lead compounds in such mouse models, thereby reducing costs and animals needed for drug development. Finally, these MCLS cultures can further contribute to the development of even more complex *in vitro* models by introducing flow, spatial organization or combining multiple organ models to study systemic interactions.

In conclusion, we developed a robust 3D *in vitro* spheroid model using freshly isolated primary mouse hepatocytes, HSCs, LSECs and KCs where all cell types are integrated and functional. More importantly, these MCLS cultures can faithfully model drug-induced fibrosis, NAFLD and NASH and can therefore be used as an *in vitro* drug screening model or for mechanistic research into disease development and progression.

4. Materials and methods

4.1. Animals

All animal experiments were carried out in the accordance with the ARRIVE guidelines and received approval by the Animal care and the Ethical Committee of animal experimentation of the Vrije Universiteit Brussel (18-212-1, 20-212-5). The institutional guidelines for the use of laboratory animals in research were strictly followed. Animals were housed in controlled temperature, 14 h light 10 h dark cycle, controlled

humidity rooms and allowed food and water ad libitum. All mice used were BALB/c aged 10–25 weeks with an average weight of ±31 g. Mice were supplied by Charles River Laboratories International, Inc.

4.2. Isolation and culturing of primary mouse hepatocytes, HSCs, KCs and LSECs

We used the protocols for the isolation of hepatocytes [45] and non-parenchymal cells (HSCs, KCs and LSECs) with the UFACS3 method described by Stradiot et al., 2017 [25] and eliminated Pronase from the beaker digestion step to enable the isolation of 4 viable cell types from 1 mouse. In brief, between 2 and 15 h prior to isolation, a BALB/c mouse was injected with 10 μg donkey anti-rabbit IgG Alexa fluor®647 (Thermofisher, A31573), diluted in 100 μl phosphate buffered saline (1x without calcium and magnesium, Lonza, LO BE-17-516 F), pH of 7.0. The mouse was anaesthetized with an overdose of 100 μl Dolethal (Vetoquinol) and afterwards the liver was perfused via the portal vein at a perfusion rate of 7.5 ml/min for 5 min with perfusion buffer 1 (SC1, detailed description can be found in Stradiot et al. [25]) at 37 °C until complete discoloration of the liver. Thereafter, the liver was perfused with perfusion buffer 2 (SC2, details in Stradiot et al. [25]) containing 0, 5 mg/ml Pronase E (Merck, 000000001,074,330,005) for 5 min followed by perfusion buffer 3 (SC2 containing 0.25 mg/ml Collagenase P (Roche, 11,213,873,001)). The perfused liver was removed and incubated at 37 °C for 15 min in a beaker containing SC2 buffer with 0,4 mg/ml Collagenase P and 0,001% DNase (Roche, 10,104,159,001) for further digestion. After the first 5 min a drop of 1 M NaOH (pH 14) was added. The resulting single cell suspension was filtered through a metal sieve (Roth, round sieve ROTILABO, 75 mm, 0.5 mm) and centrifuged for 2 min at 50 g to separate hepatocytes from NPC. Mouse hepatocytes were further purified with a 25% Percoll gradient centrifugation step (GE Healthcare Life Science, GE17-0891-02). Cell viability was assessed to be >85% after counting with trypan blue. After red blood cell lysis of the NPC for 3 min (1x, 130-094-183, Miltenyi Biotec), HSCs, KCs and LSECs were further purified with FACS (BD FACS Aria II) based on Alexa 647 and Indo 1 (violet) dot-plots (Fig. 1A). Primary hepatocytes, HSC, KC and LSEC were seeded using a Viaflo Assist Robot (4500, Integra) in cell-repellent 96-well U-bottom plates (ThermoFisher Scientific, 174, 925) at a density of 3332 cells per well in a ratio of 1hepatocyte:2HSC:1 KC:1LSEC in 20 μl seeding medium containing Williams E Media (Gibco, A12176-01) supplemented with 10% fetal bovine serum (Tico Europe, FBSEU500), 50 mg/ml kanamycin sulphate, 10 mg/ml Sodium ampicillin, 100 U/ml PenStrep, 292 mg/ml L-glutamine and 7 ng/ml Glucagon. This procedure permits multiple isolations in one day allowing us to create separate biological repeats through the combination of parenchymal cells with non-parenchymal cells from the same mouse or from distinct mice. Cell aggregation was enhanced by gentle rotation on an orbital shaker (Infors Celltron) at a speed of 80 rpm. After 24 h, 150 μl of liver spheroid medium (LSM) containing serum free Williams E Media, 50 μg/ml kanamycin sulphate, 10 μg/ml Sodium ampicillin, 100 U/ml PenStrep, 292 mg/ml L-glutamine, 7 ng/ml Glucagon, 0,5 μg/ml insulin (I1882, Sigma-Aldrich, Belgium) and 25 μg/ml Hydrocortisone sodium succinate (Solu-CortefPharmacy) [25] was added to the forming spheroids. At day 2 of the culture, 135 μl of medium was replaced with 100 μl LSM and subsequently refreshed every 2–3 days with 100 μl LSM. Bright field images to assess spheroid morphology were taken with an Axiovert light microscope (Carl Zeiss) and EVOS (M7000, ThermoFisher Scientific).

4.3. Spheroid exposures

For cytochrome P-450 (CYP) induction, spheroids were exposed at day 3–25 μM β-naphthoflavone (Sigma Aldrich, N3633-1G) and 10 μM Rifampicin (Merck, R7382-1G) for 24 h. For direct HSC activation, spheroids were exposed to 10 ng/ml TGFβ (Peprotech Inc, 100-21C) for 72 h at day 4. For the assessment of KC functionality, LPS (Sigma Aldrich, L4391) (100 ng/ml) was added for 72 h to spheroids with or without KCs at day 4. For cytokine treatment, spheroids were exposed to IL-1β (50 ng/ml), TNFα (100 ng/ml) or IL-1β (50 ng/ml) and TNFα (100 ng/ml) for 72 h at day 4 in LSM. 6 spheroids per condition for each biological replicate were collected for RNA analysis and media was collected for further analysis.

4.4. Induction of fibrosis, NAFLD and NASH

After 7 days of culture fibrosis was induced by exposure to APAP (Sigma Aldrich, A7302) at a concentration of 1.25 mM for 72 h. Control spheroids were kept in media containing 0.2% DMSO (Sigma Aldrich, D2650). 6 spheroids per condition for each biological replicate were collected for mRNA analysis and media was collected for further analysis. No media refreshments were performed to allow the accumulation of Collagen 6 in the media. NAFLD conditions were established by the addition of free fatty acids (FFA): unsaturated oleic acid (Sigma Aldrich, O1005) and saturated palmitic acid (Sigma Aldrich, P-5585) that were solubilized in ethanol and added to the LSM in a concentration of 400 μM oleic acid and 500 μM palmitic acid. Spheroids were exposed to FFA rich media from day 7 until day 17 with media refreshment every 2–3 days. Control spheroids were kept in media containing the FFA solvent (ethanol). For NASH induction, LPS (100 ng/ml) was added to the FFA rich media from day 14 until day 17 without media refreshment.

4.5. Exposure to anti-NAFLD/NASH drugs

Peroxisome proliferator-activated receptor (PPAR) agonists: Pioglitazone (30 μM) (Sigma-Aldrich, CDS021593), Elafibranor (30 μM) (MedChemExpress, HY-16737) and Lanifibranor (10 μM, MedChemExpress,HY-104049)), the ASK-1 inhibitor Selonsertib (10 μM, MedChemExpress, HY-18938) and the FXR agonist Obeticholic acid (50 μM, MedChemExpress, HY-12222) were added to spheroids in NAFLD conditions from day 7 until day 17 to assess the effect on steatosis and on spheroids in NASH conditions from day 15 until day 17 to assess their effect on fibrosis reduction.

4.6. mRNA analysis

6 spheroids per condition were lysed and total mRNA was extracted using the ReliaPrep RNA Cell Miniprep System (Promega, 1,074,308). mRNA was then reverse transcribed into cDNA using the MLV reverse transcriptase (Promega, M1701). qPCR was performed using GoTaq qPCR Master Mix with BRYTE green (Promega, A6002) and measured using a Quantstudio3 Fast PCR system (ThermoFisher, A28567). Analysis was performed according to the comparative Ct (ΔΔCt) method where each Ct value was normalized to the reference gene *Gtf2b*. When HSC activation was induced, each Ct value was normalized to the mean of the reference gene *Gft2b* with *Desmin*. Gene specific primers (Suppl. Table 1) were used and manufactured by Integrated DNA Technologies.

4.7. Cell viability

ATP was measured with a luciferase-based ATP measurement protocol following the manufacturer's instructions (CellTiter Glo Luminescent Cell Viability Assay Kit) (Promega, G7571). After exposure to APAP, spheroids were individually transferred in 100 μl media to a black bottom 96-well plate, and an equal volume of ATP substrate was added to the spheroids. After a 10 min incubation at room temperature on a shaker and 10 min of the shaker, luminescence was measured using a GloMax (Promega, GM3000).

4.8. Immunostaining

Spheroids were rinsed with PBS, fixed in 10% formalin for 10 min at room temperature, washed 3 times with PBS and stored at 4 °C. For

Table 1
Genetic sequences of used primers.

Gene	Sequence 5′-3′
Adgre1(F4/80) forward	CCTGGACGAATCCTGTGAAG
Adgre1(F4/80) reverse	GGTGGGACCACAGAGAGTTG
Acta2 forward	CCAGCACCATGAAGATCAAG
Acta2 reverse	TGGAAGGTAGACAGCGAAGC
Col1a1 forward	GCTCCTCTTAGGGGCCACT
Col1a1 reverse	CCACGTCTCACCATTGGGG
Col6a3 forward	AAGGGAAGCATCGGGAAC
Col6a3 reverse	CCCATCTCTCCCGTCATCT
Cyp1a1 forward	CAATGAGTTTGGGGAGGTTACTG
Cyp1a1 reverse	CCCTTCTCAAATGTCCTGTAGTG
Cyp3a11 forward	TGAATATGAAACTTGCTCTCACTAAAA
Cyp3a11 reverse	CCTTGTCTGCTTAATTTCAGAGGT
Desmin forward	GCCACCTACCGGAAGCTACT
Desmin reverse	GCAGAGAAGGTCTGGATAGGAA
Gtf2b forward	ATTGGCAAGGGTACAGGAGC
Gtf2b reverse	GAGGTTGATTCTGTCCGCCA
Il-1β forward	GAAATGCCACCTTTTGACAGTG
Il-1β reverse	TGGATGCTCTCATCAGGACAG
Lox forward	TGTACGCTGTGACATTCGCT
Lox reverse	CACTGGGAACTGGGCTTCTT
Lyve1 forward	CAGCACACTAGCCTGGTGTTA
Lyve1 reverse	CGCCCATGATTCTGCATGTAGA
Tgfβ forward	TGGAGCAACATGTGGAACTC
Tgfβ reverse	GTCAGCAGCCGGTTACCA
Tnfα forward	TCTTCTCATTCCTGCTTGTGG
Tnfα reverse	GGTCTGGGCCATAGAACTGA

immunohistochemistry staining, spheroids were paraffin embedded and cut into 5 μm thin sections using a microtome (Microm, HM340E). For immunofluorescent staining, spheroids were stained as whole spheroids or were paraffin embedded and sliced into 5 μm thick sections. Staining procedures are fully described by Stradiot et al., 2017 [25] and Leite et al., 2016 [33]. Antibodies and concentration details are provided in Suppl. Table 2. Quantification of Collagen 1 immunofluorescent staining was done with Orbit on 4–6 spheroids of 2–4 different cultures.

4.9. Electron microscopy

Spheroids were rinsed with PBS and fixed in 4% Formaldehyde (Sigma-Aldrich, F8776) and 2.5% Glutaraldehyde (Sigma-Aldrich, G6257) in PHEM buffer (60 mM PIPES (Sigma-Aldrich, p6757), 21 mM HEPES (Merck Group, H4034), 10 mM EGTA (Merck Group, E4378), 2 mM $MgCl_2$·6H2O (Merck Group, M2393) and 684.5 mM NaCl (Merck Group, S5886) and 6.95 pH) for 24 h at 4 °C. Samples were stored in PBS until processing. Processing was done by 1 h treatment with freshly made 1% tannic acid in PHEM buffer and 1 h treatment of 1% OsO4 in H_2O. Samples were dehydrated in an ethanol gradient (30%, 60%, 90% for 5 min each, 5 times for 4 min in 100% ethanol), incubated twice for 10 min in hexamethyldisilane and left to evaporate overnight. Before imaging, samples were mounted on metal stubs using carbon tape and were sputter coated with 10 nm gold/palladium. Imaging was performed with a commercial scanning electron microscopy (SEM) system (Gemini, Zeiss) with a 2 kV electron beam.

Table 2
Antibodies used for immunofluorescence and immunohistochemistry.

Antibody	Manufacturer & Catalogue number	Dilution
Anti-HNF4α	Abcam, ab41898	1/200
Anti-HNF4α (DAB)	SantaCruz, SC-8987	1/100
Anti-Desmin	Thermo Fisher Scientific, RB-9014-P1	1/200
Anti-LYVE1	R&D systems (via Bio-Techne), AF2125	1/100
Anti-CD68	AbD Serotec (via Bio-Rad), MCA1957GA	1/100
Anti-F4/80	AbD Serotec (via Bio-Rad), MCA497GA	1/200
Anti-Col1	Abcam, ab270993	1/500
Anti-Col1	Abcam, ab21286	1/300
Donkey anti-Rabbit	Invitrogen (via Thermo Fisher Scientific), A31573	1/200
Donkey anti-Mouse	Abcam, ab175658	1/200
Donkey anti-Goat	Thermo Scientific, A11055	1/200
Donkey anti-Rabbit	Thermo Scientific, A-21207	1/200
Donkey anti-Rabbit	Jackson Immuno Research, 711-166-152	1/200
Donkey anti-Rat	Abcam, ab150155	1/200
HRP-conjugated rabbit anti-Rat	Thermo Scientific, 61-9520	1/200
HRP-conjugated anti-Rabbit	Dako, K400311-2	–
HRP-conjugated rabbit anti-Goat	Dako, P044901-02	1/200

4.10. BODIPY staining

Fixed spheroids stored at 4 °C were washed with PBS and stained with BODIPY staining dye 493/503 (15 mM diluted January 2000 in PBS (Life Technologies, D3922)) for 40 min at room temperature. Spheroids were washed 3x with PBS and mounted with Mowiol (Merck, 81,381) containing 1/1000 DAPI (Sigma-Aldrich, D9564). Quantification was performed on whole spheroid stainings of 4–6 individual spheroids of 3 different cultures with FIJI ((https://imagej.net/software/fiji/).

4.11. Albumin, collagen 6 and cytokine ELISA

Albumin secretion into the media of 2D and 3D cultures was analyzed using an Albumin ELISA (MyBioSource, MBS2516177). 2D hepatocytes were cultured on rat tail collagen (Corning, 354,236) coated wells (57,000/cm^2) in LSM. At day 4, culture media was collected from 2D hepatocyte cultures. At day 4, 7 and 14 culture media from 6 individual spheroids was pooled. Collected media was centrifuged at 1300 rpm for 8 min to remove debris. Albumin was determined using a plate reader (BioRad, iMark) by O.D. extrapolation from a standard curve and the amount was calculated per 1000 cells per 24 h. Collagen 6 secretion into the media was measured using a Collagen 6 ELISA (MyBioSource, MBS2704928). The media from 6 individual spheroids, treated for 72 h with Ctrl, 1.25 mM APAP or 10 ng/ml TGFβ, was pooled and centrifuged at 1300 rpm for 8 min. Collagen 6 content was determined using a plate reader (BioRad, iMark) by O.D. extrapolation from the standard curve. Cytokine secretion into the media was measured using the GeniePlex Mouse Inflammation 5-Plex Panel 1 (AssayGenie, MOAMPM016). The media from 6 individual spheroids, treated for 72 h with Ctrl or LPS (100 ng/ml), was pooled and centrifuged at 1300 rpm for 8 min. Cytokine concentration was determined using a BD FACS Aria II and by O.D. extrapolation from the standard curves.

4.12. Statistics

All statistical tests (non-parametric) were performed with Graphpad Prism 9.0. Wilcoxon test (1 tailed) was used for a 2 paired group comparison when MCLS cultures were treated with APAP. Friedman's test (1 tailed) was used with multiple paired groups together with a Dunnett test when MCLS cultures were treated with a certain compound or had a certain cellular composition. Mann-Whitney test (1 tailed) was used for a 2 group comparison (Collagen stainings or albumin measurements). Kruskal-Wallis (1 tailed) test was used (addition of inflammatory cytokines, Collagen and BODIPY stainings) with multiple groups together with a Dunnett test when MCLS cultures were treated with a certain compound. Symbols meaning: *P $\leq$ 0.05, **P $\leq$ 0.01, ***P $\leq$ 0.001, ****P $\leq$ 0.0001.

Funding statement

EO was supported by "Wetenschappelijk Fonds Willy Gepts" of the UZ Brussel (WFWG20-23). LC was supported by the Vrije Universiteit Brussel. SV was supported by Fund of Scientific Research Flanders (FWO–V) junior post-doctoral fellowship (1243121N). IM was supported by FWO–V senior post-doctoral fellowship (12N5419N and 1509220N). The work was supported by the grant awarded to PM and

LG of the European Union's Horizon 2020 research and innovation program under the Marie Sklodowska-Curie Grant Agreement No. 766181, project DeLIVER. Additionally, the work was supported by grants awarded to LG by FWO-V (G042719 N) and IBOF Vlaamse Regering 2021.

Authors contributions

Elise Anne van Os: Conceptualization, Investigation, Methodology, Formal analysis, Validation, Visualization, Data curation, Writing-Original Draft. **Laura Cools**: Conceptualization, Investigation, Methodology, Formal analysis, Validation, Visualization, Data curation, Writing- Original Draft. **Nathalie Eysackers**: Data curation, Methodology, Formal analysis, Investigation **Karolina Szafrańska:** Methodology, Formal analysis, Investigation, **Stefaan Verhulst**: Methodology, Conceptualization, Formal analysis, Writing review & editing. **Ayla Smout**: Methodology, Formal analysis. **Hendrik Reynaert:** Funding acquisition, Writing review & editing. **Peter McCourt:** Investigation, Funding acquisition, Writing - review & editing. **Inge Mannaerts**: Investigation, Conceptualization, Supervision, Writing review & editing. **Leo A. van Grunsven**: Conceptualization, Funding acquisition, Supervision, Writing - review & editing.

Declaration of competing interest

The authors declare that they have no known competing financial interests or personal relationships that could have appeared to influence the work reported in this paper.

Data availability

Data will be made available on request.

Acknowledgements

The authors would like to thank Randi Olsen and Tom-Iver Eilertsen from Advanced Microscopy Core Facility at the University of Tromsø for the electron microscopy expertise. In addition, the authors would like to thank Jean-Marc Lazou for performing flow cytometry cell sorting. Schemes were created with BioRender.com.

Appendix A. Supplementary data

Supplementary data to this article can be found online at https://doi.org/10.1016/j.biomaterials.2022.121817.

References

[1] S.K. Asrani, H. Devarbhavi, J. Eaton, P.S. Kamath, Burden of liver diseases in the world, J. Hepatol. 70 (1) (2019) 151–171.
[2] S. Lemoinne, S.L. Friedman, New and emerging anti-fibrotic therapeutics entering or already in clinical trials in chronic liver diseases, Curr. Opin. Pharmacol. 49 (2019) 60–70.
[3] Y.A. Lee, M.C. Wallace, S.L. Friedman, Pathobiology of liver fibrosis: a translational success story, Gut 64 (5) (2015) 830–841.
[4] C.K. Negi, P. Babica, L. Bajard, J. Bienertova-Vasku, G. Tarantino, Insights into the molecular targets and emerging pharmacotherapeutic interventions for nonalcoholic fatty liver disease, Metabolism 126 (2022), 154925.
[5] S.A. Polyzos, E.S. Kang, C. Boutari, E.-J. Rhee, C.S. Mantzoros, Current and emerging pharmacological options for the treatment of nonalcoholic steatohepatitis, Metabolism 111 (2020), 154203.
[6] G. Xie, X. Wang, L. Wang, L. Wang, R.D. Atkinson, G.C. Kanel, et al., Role of differentiation of liver sinusoidal endothelial cells in progression and regression of hepatic fibrosis in rats, Gastroenterology 142 (4) (2012) 918–927 e6.
[7] G. Kolios, V. Valatas, E. Kouroumalis, Role of Kupffer cells in the pathogenesis of liver disease, World J. Gastroenterol.: WJG 12 (46) (2006) 7413.
[8] S.L. Friedman, M. Pinzani, Hepatic fibrosis 2022: unmet needs and a blueprint for the future, Hepatology 75 (2) (2022) 473–488.
[9] L.A. van Grunsven, 3D in vitro models of liver fibrosis, Adv. Drug Deliv. Rev. 121 (2017) 133–146.
[10] P.-A. Soret, J. Magusto, C. Housset, J. Gautheron, In vitro and in vivo models of non-alcoholic fatty liver disease: a critical appraisal, J. Clin. Med. 10 (1) (2021) 36.
[11] Y. Popov, D. Schuppan, Targeting liver fibrosis: strategies for development and validation of antifibrotic therapies, Hepatology 50 (4) (2009) 1294–1306.
[12] T. Tao, P. Deng, Y. Wang, X. Zhang, Y. Guo, W. Chen, et al., Microengineered multi-organoid system from hiPSCs to recapitulate human liver-islet Axis in normal and type 2 diabetes, Adv. Sci. 9 (5) (2022), e2103495.
[13] A. Baze, C. Parmentier, D.F.G. Hendriks, T. Hurrell, B. Heyd, P. Bachellier, et al., Three-dimensional spheroid primary human hepatocytes in monoculture and coculture with nonparenchymal cells, Tissue Eng. C Methods 24 (9) (2018) 534–545.
[14] J. Shiota, L.C. Samuelson, N. Razumilava, Hepatobiliary organoids and their applications for studies of liver health and disease: are we there yet? Hepatology 74 (4) (2021) 2251–2263.
[15] K. Zeilinger, N. Freyer, G. Damm, D. Seehofer, F. Knöspel, Cell sources for in vitro human liver cell culture models, Exp. Biol. Med. 241 (15) (2016) 1684–1698.
[16] T. Hurrell, V. Kastrinou-Lampou, A. Fardellas, D.F. Hendriks, Nordling Å, I. Johansson, et al., Human liver spheroids as a model to study aetiology and treatment of hepatic fibrosis, Cells 9 (4) (2020) 964.
[17] M. Zabulica, T. Jakobsson, F. Ravaioli, M. Vosough, R. Gramignoli, E. Ellis, et al., Gene editing correction of a urea cycle defect in organoid stem cell derived hepatocyte-like cells, Int. J. Mol. Sci. 22 (3) (2021) 1217.
[18] B. Lucendo-Villarin, J. Meseguer-Ripolles, J. Drew, L. Fischer, E. Ma, O. Flint, et al., Development of a cost-effective automated platform to produce human liver spheroids for basic and applied research, Biofabrication 13 (1) (2020), 015009.
[19] T. Tricot, C.M. Verfaillie, M. Kumar, Current status and challenges of human induced pluripotent stem cell-derived liver models in drug discovery, Cells 11 (3) (2022) 442.
[20] E. Stengelin, J. Thiele, S. Seiffert, Multiparametric material functionality of microtissue-based in vitro models as alternatives to animal testing, Adv. Sci. (2022), e2105319.
[21] M.J. Prescott, K. Lidster, Improving quality of science through better animal welfare: the NC3Rs strategy, Lab. Anim. 46 (4) (2017) 152–156.
[22] K. Elvevold, B. Smedsrød, I. Martinez, The liver sinusoidal endothelial cell: a cell type of controversial and confusing identity, Am. J. Physiol. Gastrointest. Liver Physiol. 294 (2) (2008) G391–G400.
[23] G. Elaut, T. Henkens, P. Papeleu, S. Snykers, M. Vinken, T. Vanhaecke, et al., Molecular mechanisms underlying the dedifferentiation process of isolated hepatocytes and their cultures, Curr. Drug Metabol. 7 (6) (2006) 629–660.
[24] I. Mannaerts, S.B. Leite, S. Verhulst, S. Claerhout, N. Eysackers, L.F.R. Thoen, et al., The Hippo pathway effector YAP controls mouse hepatic stellate cell activation, J. Hepatol. 63 (3) (2015) 679–688.
[25] L. Stradiot, S. Verhulst, T. Roosens, C.I. Oie, I.M. Moya, G. Halder, et al., Functionality based method for simultaneous isolation of rodent hepatic sinusoidal cells, Biomaterials 139 (2017) 91–101.
[26] I. Mannaerts, N. Eysackers, E. Anne van Os, S. Verhulst, T. Roosens, A. Smout, et al., The fibrotic response of primary liver spheroids recapitulates in vivo hepatic stellate cell activation, Biomaterials 261 (2020), 120335.
[27] V.C. Cogger, J.N. O'Reilly, A. Warren, D.G. Le Couteur, A standardized method for the analysis of liver sinusoidal endothelial cells and their fenestrations by scanning electron microscopy, JoVE 98 (2015), e52698.
[28] J.-B. Soares, P. Pimentel-Nunes, R. Roncon-Albuquerque, A. Leite-Moreira, The role of lipopolysaccharide/toll-like receptor 4 signaling in chronic liver diseases, Hepatology International 4 (4) (2010) 659–672.
[29] E. Seki, S. De Minicis, C.H. Österreicher, J. Kluwe, Y. Osawa, D.A. Brenner, et al., TLR4 enhances TGF-β signaling and hepatic fibrosis, Nat. Med. 13 (2007) 1324.
[30] S. Bhandari, R. Li, J. Simón-Santamaría, P. McCourt, S.D. Johansen, B. Smedsrød, et al., Transcriptome and proteome profiling reveal complementary scavenger and immune features of rat liver sinusoidal endothelial cells and liver macrophages, BMC Molecular and Cell Biology 21 (1) (2020) 85.
[31] J.-P. Pradere, J.S. Troeger, D.H. Dapito, A.A. Mencin, R.F. Schwabe, Toll-like receptor 4 and hepatic fibrogenesis, Semin. Liver Dis. 30 (3) (2010) 232–244.
[32] S. Kumar, J. Wang, S.K. Shanmukhappa, C.R. Gandhi, Toll-like receptor 4–independent carbon tetrachloride–induced fibrosis and lipopolysaccharide-induced acute liver injury in mice: role of hepatic stellate cells, Am. J. Pathol. 187 (6) (2017) 1356–1367.
[33] S.B. Leite, T. Roosens, A. El Taghdouini, I. Mannaerts, A.J. Smout, M. Najimi, et al., Novel human hepatic organoid model enables testing of drug-induced liver fibrosis in vitro, Biomaterials 78 (2016) 1–10.
[34] Q. Bai, H. Yan, Y. Sheng, Y. Jin, L. Shi, L. Ji, et al., Long-term acetaminophen treatment induced liver fibrosis in mice and the involvement of Egr-1, Toxicology 382 (2017) 47–58.
[35] A.K. Leamy, R.A. Egnatchik, J.D. Young, Molecular mechanisms and the role of saturated fatty acids in the progression of non-alcoholic fatty liver disease, Prog. Lipid Res. 52 (1) (2013) 165–174.
[36] S. Srivastava, C. Chan, Hydrogen peroxide and hydroxyl radicals mediate palmitate-induced cytotoxicity to hepatoma cells: relation to mitochondrial permeability transition, Free Radic. Res. 41 (1) (2007) 38–49.
[37] J.P. Allard, E. Aghdassi, S. Mohammed, M. Raman, G. Avand, B.M. Arendt, et al., Nutritional assessment and hepatic fatty acid composition in non-alcoholic fatty liver disease (NAFLD): a cross-sectional study, J. Hepatol. 48 (2) (2008) 300–307.
[38] A.M. van den Hoek, L. Verschuren, M.P.M. Caspers, N. Worms, A.L. Menke, H.M. G. Princen, Beneficial effects of elafibranor on NASH in E3L.CETP mice and differences between mice and men, Sci. Rep. 11 (1) (2021) 5050.
[39] B. Shen, L.G. Lu, Efficacy and safety of drugs for nonalcoholic steatohepatitis, J Dig Dis 22 (2) (2021) 72–82.

[40] P.J. Hsiao, H.C. Chiou, H.J. Jiang, M.Y. Lee, T.J. Hsieh, K.K. Kuo, Pioglitazone enhances cytosolic lipolysis, β-oxidation and autophagy to ameliorate hepatic steatosis, Sci. Rep. 7 (1) (2017) 9030.
[41] S.A. Harrison, V.W. Wong, T. Okanoue, N. Bzowej, R. Vuppalanchi, Z. Younes, et al., Selonsertib for patients with bridging fibrosis or compensated cirrhosis due to NASH: results from randomized phase III STELLAR trials, J. Hepatol. 73 (1) (2020) 26–39.
[42] M.C. Morrison, L. Verschuren, K. Salic, J. Verheij, A. Menke, P.Y. Wielinga, et al., Obeticholic acid modulates serum metabolites and gene signatures characteristic of human NASH and attenuates inflammation and fibrosis progression in Ldlr-/-.Leiden mice, Hepatol Commun 2 (12) (2018) 1513–1532.
[43] C.C. Bell, A.C.A. Dankers, V.M. Lauschke, R. Sison-Young, R. Jenkins, C. Rowe, et al., Comparison of hepatic 2D sandwich cultures and 3D spheroids for long-term toxicity applications: a multicenter study, Toxicol. Sci. 162 (2) (2018) 655–666.
[44] S. Lefere, T. Puengel, J. Hundertmark, C. Penners, A.K. Frank, A. Guillot, et al., Differential effects of selective- and pan-PPAR agonists on experimental steatohepatitis and hepatic macrophages, J. Hepatol. 73 (4) (2020) 757–770.
[45] L.A. Gonçalves, A.M. Vigário, C. Penha-Gonçalves, Improved isolation of murine hepatocytes for in vitro malaria liver stage studies, Malar. J. 6 (2007) 169.
[46] R. Nudischer, K. Renggli, A. Hierlemann, A.B. Roth, C. Bertinetti-Lapatki, Characterization of a long-term mouse primary liver 3D tissue model recapitulating innate-immune responses and drug-induced liver toxicity, PLoS One 15 (7) (2020), e0235745.
[47] J. Bonnardel, W. T'Jonck, D. Gaublomme, R. Browaeys, C.L. Scott, L. Martens, et al., Stellate cells, hepatocytes, and endothelial cells imprint the kupffer cell identity on monocytes colonizing the liver macrophage niche, Immunity 51 (4) (2019) 638–654, e9.
[48] A.A. Kolodziejczyk, S. Federici, N. Zmora, G. Mohapatra, M. Dori-Bachash, S. Hornstein, et al., Acute liver failure is regulated by MYC- and microbiome-dependent programs, Nat. Med. 26 (12) (2020) 1899–1911.
[49] M. Guilliams, J. Bonnardel, B. Haest, B. Vanderborght, C. Wagner, A. Remmerie, et al., Spatial proteogenomics reveals distinct and evolutionarily conserved hepatic macrophage niches, Cell 185 (2) (2022) 379–396, e38.
[50] S. Dimova, T. Stoytchev, Influence of rifampicin on the toxicity and the analgesic effect of acetaminophen, Eur. J. Drug Metab. Pharmacokinet. 19 (4) (1994) 311–317.
[51] R.E. Feaver, B.K. Cole, M.J. Lawson, S.A. Hoang, S. Marukian, B.R. Blackman, et al., Development of an in vitro human liver system for interrogating nonalcoholic steatohepatitis, JCI Insight 1 (20) (2016), e90954.
[52] C.P. Day, O.F. James, Steatohepatitis: a tale of two "hits, Gastroenterology 114 (4) (1998) 842–845.
[53] K.S. Tølbøl, M.N. Kristiansen, H.H. Hansen, S.S. Veidal, K.T. Rigbolt, M.P. Gillum, et al., Metabolic and hepatic effects of liraglutide, obeticholic acid and elafibranor in diet-induced obese mouse models of biopsy-confirmed nonalcoholic steatohepatitis, World J. Gastroenterol. 24 (2) (2018) 179–194.
[54] F. Briand, C. Heymes, L. Bonada, T. Angles, J. Charpentier, M. Branchereau, et al., A 3-week nonalcoholic steatohepatitis mouse model shows elafibranor benefits on hepatic inflammation and cell death, Clin Transl Sci 13 (3) (2020) 529–538.
[55] G. Wettstein, J.M. Luccarini, L. Poekes, P. Faye, F. Kupkowski, V. Adarbes, et al., The new-generation pan-peroxisome proliferator-activated receptor agonist IVA337 protects the liver from metabolic disorders and fibrosis, Hepatol Commun 1 (6) (2017) 524–537.
[56] A.J. Sanyal, N. Chalasani, K.V. Kowdley, A. McCullough, A.M. Diehl, N.M. Bass, et al., Pioglitazone, vitamin E, or placebo for nonalcoholic steatohepatitis, N. Engl. J. Med. 362 (18) (2010) 1675–1685.
[57] G.R. Budas, S.K. Karnik, T. Jonnson, T.B. Shafizadeh, S.M. Watkins, D. G. Breckenridge, et al., Reduction of liver steatosis and fibrosis with an Ask1 inhibitor in a murine model of nash is accompanied by improvements in cholesterol, bile acid and lipid metabolism, J. Hepatol. 64 (2016).